Spectral imaging of time-resolved anisotropy: theory and experiment

Yanzhou Zhou (周延周)*, Qingruo Wang (王钦若), Jingsong He (何竞松), and Lerong Lin (林乐荣)

Faculty of Automation, Guangdong University of Technology, Guangzhou 510006, China

**E-mail: zhouyanzhou@hotmail.com*

Received June 23, 2010

Time-resolved fluorescence anisotropy on the nanosecond time scale is useful for the study of the rapid rotation of macromolecules. A system combining the capabilities of fluorescence spectral imaging with time-resolved fluorescence anisotropy and enabling the wide-field measurement of the spectroscopic parameters of fluorophores is discussed. The phasor approach is used to quantitatively analyze the time-resolved fluorescence anisotropy by transforming the polarized parallel and perpendicular components to the phasor space in the frequency domain, respectively, and a unique way to calculate the fluorescence rotational correlation time is put forward. Experimental results prove that the phasor approach is a proper model for the time-resolved fluorescence anisotropy.

OCIS codes: 170.2520, 170.3650, 170.6280.

doi: 10.3788/COL20100810.0937.

Time-resolved fluorescence depolarization on the nanosecond time scale is a powerful technique for the study of the rapid rotations of molecules in liquids. The basic idea is that a fluorophore excited by polarized light will also emit polarized light. If the fluorophore is moving, the fluorescence tends to "be depolarized". The "depolarized" effect is the greatest with fluorophores freely tumbling in solution[1,2]. By using pulsed or modulated light sources and gated controlled intensified camera, we can use traditional wide field microscopy to visualize the distribution of the fluorescence anisotropy or the "depolarized" effect in the complex biological system pixel by pixel[1−6].

Measurements of fluorescence lifetime normally consist of a light source and a detector. A series of images are collected while the time or phase delay is shifted between the excitation source and the detector. This can be extended to the time-resolved anisotropy measurement by providing a polarized excitation source and collecting two sets of images. The first set is collected with an excitation polarizer oriented parallel to the analyzing polarizer and the second set with it oriented perpendicular. If N images are collected in each series, and each image collected is a spectral image (x, λ), and then the intensity data can be indexed as $p_{\parallel}(x, \lambda, n)$ and $p_{\perp}(x, \lambda, n)$, where n is an index running from 1 to N, x is the slot width of the spectrograph, λ is the wavelength, and the subscript $\parallel$ or $\perp$ refers to the orientation of the analyzing polarizer. To obtain a time-resolved spectral image, the parallel and perpendicular images are summed, $p_{\rm s}(x, \lambda, n) = p_{\parallel}(x, \lambda, n) + 2p_{\perp}(x, \lambda, n)$[1,6]. The time-resolved anisotropy $r(x, \lambda, n)$ with an exponential tail can also be presented as the function of parallel and perpendicular components[1,6]:

$$\begin{aligned} r(x,\lambda,n) &= \frac{p_{\parallel}(x,\lambda,n) - p_{\perp}(x,\lambda,n)}{p_{\parallel}(x,\lambda,n) + 2p_{\perp}(x,\lambda,n)} \\ &= [r_0(x,\lambda) - r_{\infty}(x,\lambda)] \cdot \exp\left[-\frac{n}{\theta(x,\lambda)}\right] \\ &\quad + r_{\infty}(x,\lambda), \\ p_{\rm s}(x,\lambda,n) &= p_0(x,\lambda) \cdot \exp\left[-\frac{n}{\tau(x,\lambda)}\right], \end{aligned} \tag{1}$$

where r_0 is the fundamental anisotropy, r_{∞} is the infinite anisotropy, θ is the molecule rotational correlation time, τ is the fluorescence lifetime, and $p_0(x, \lambda) = p_{\rm s}(x, \lambda, 0)$. If we define the fluorescence joint time ξ as

$$\frac{1}{\xi(x,\lambda)} = \frac{1}{\tau(x,\lambda)} + \frac{1}{\theta(x,\lambda)}, \tag{2}$$

Eqs. (1) and (2) form the system of the linear equations. Their roots can be rewritten as

$$\begin{aligned} p_{\parallel}(x,\lambda,n) &= \frac{p_0(x,\lambda)}{3} \cdot \left\{ 2\left[r_0(x,\lambda) - r_{\infty}(x,\lambda)\right] \cdot \exp\left[-\frac{n}{\xi(x,\lambda)}\right] + \left[1 + 2r_{\infty}(x,\lambda)\right] \cdot \exp\left[-\frac{n}{\tau(x,\lambda)}\right] \right\}, \\ p_{\perp}(x,\lambda,n) &= \frac{p_0(x,\lambda)}{3} \cdot \left\{ \left[1 - r_{\infty}(x,\lambda)\right] \cdot \exp\left[-\frac{n}{\tau(x,\lambda)}\right] - \left[r_0(x,\lambda) - r_{\infty}(x,\lambda)\right] \cdot \exp\left[-\frac{n}{\xi(x,\lambda)}\right] \right\}. \end{aligned} \tag{3}$$

It is noted that neither $p_{\parallel}$ nor $p_{\perp}$ is single exponential decay, but bi-exponential process, represented by the points inside and outside the semicircle in the phasor space, respectively[7−10]. From Eq. (3), we obtain

$$\begin{aligned} \Delta p(x,\lambda,n) &= r(x,\lambda,n) \cdot p_{\rm s}(x,\lambda,n) \\ &= p_0(x,\lambda) \cdot \left\{ \left[r_0(x,\lambda) - r_{\infty}(x,\lambda)\right] \cdot \exp\left[-\frac{n}{\xi(x,\lambda)}\right] + r_{\infty}(x,\lambda) \cdot \exp\left[-\frac{n}{\tau(x,\lambda)}\right] \right\}. \end{aligned} \tag{4}$$

If $r_\infty = 0$, $\triangle p$ is a single exponential decay with the time constant ξ defined in Eq. (2), represented by a point on the semicircle in the phasor space[7,8,10]. For the case of $r_\infty \neq 0$, it is a point by the linear interpolation between the point (0, 0) and the point representing fluorescence joint time ξ weighted by r_∞ and $(r_0 - r_\infty)$ in the phase space, respectively.

In Refs. [3,6], the parallel and perpendicular image data are separately Fourier transformed to $P_{\parallel,\perp}(x, \lambda, \omega)$, and the frequency-dependent anisotropy $r(x, \lambda, \omega)$ and the phase difference $\Delta\phi(x, \lambda, \omega)$ are computed by

$$\widetilde{r}(x,\lambda,\omega) = \frac{\left|P_\parallel(x,\lambda,\omega)\right| - \left|P_\perp(x,\lambda,\omega)\right|}{\left|P_\parallel(x,\lambda,\omega)\right| + 2\left|P_\perp(x,\lambda,\omega)\right|}, \quad (5)$$

$$\phi_{\parallel,\perp}(x,\lambda,\omega) = \tan^{-1}\left[\frac{\mathrm{Im}\left(P_{\parallel,\perp}(x,\lambda,\omega)\right)}{\mathrm{Re}\left(P_{\parallel,\perp}(x,\lambda,\omega)\right)}\right],$$

$$\Delta\phi(x,\lambda,\omega) = \phi_\parallel(x,\lambda,\omega) - \phi_\perp(x,\lambda,\omega). \quad (6)$$

When $\widetilde{r}$ is evaluated using the zero frequency coefficients, it yields r_{DC}; when ω is evaluated using a single modulated frequency $\omega_0 = 2\pi f$, r_{AC} results. The rotational correlation time θ can be computed from the viscosity η, the hydrodynamic volume V, the gas constant R, and the absolute temperature T:

$$\theta = \frac{\eta V}{RT}. \quad (7)$$

Equations (5) and (6) are the basestone of the measurement of the time-resolved anisotropy in the frequency domain[3,6], and are just suitable for a spherical rotator. However, in a complex situation the decay of anisotropy is not single exponential since the motion of a molecule occurs along different axes with different rates[1]. Because infinite anisotropy gives a contribution to the polarization, and cannot be eliminated *a priori*, we can easily find that Eq. (5) is not the Fourier transform of the time-resolved anisotropy according to Eq. (1), and r_{AC} is not the anisotropy at the modulated frequency f. This is the reason that the relation of r_{AC} from Eq. (5) and viscosity does not conform to the Perrin equation[6]. The best way to quantitatively analyze the time-resolved anisotropy and calculate the rotational correlation time without prerequisite is the phasor approach deduced from the difference between the parallel and perpendicular components according to Eq. (4). Another advantage is to dodge the division which often causes ill-posed errors at the tail of the time-resolved anisotropy.

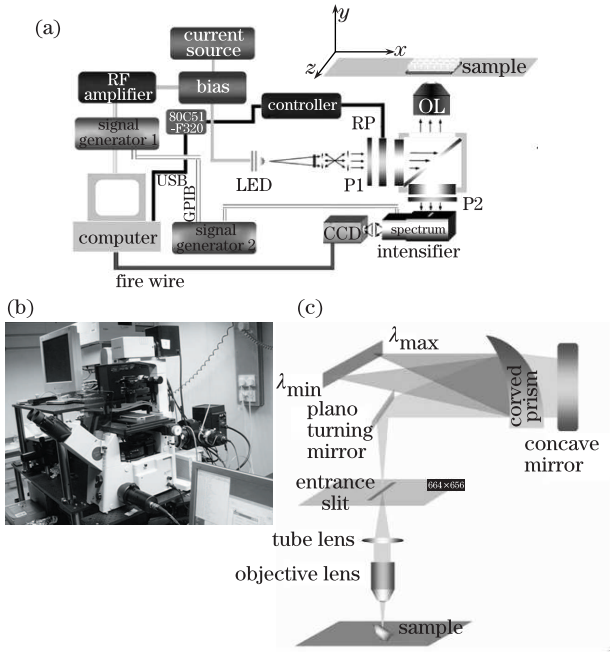

Fig. 1. Experimental system (rsFLIM) configuration. (a) Schematic of rsFLIM; (b) photo of rsFLIM; (c) schematic of the spectrograph.

In order to verify the theoretical model, the experimental system (rsFLIM) was built as an add-on to an inverted microscope, as shown in Figs. 1(a) and (b)[6]. The microscope was illuminated using light emitting diodes (LEDs). After passing through a polarizer, the linearly polarized light was directed into a liquid crystal display (LCD) polarization rotator, which rotated the polarization either 0° or 90° directly under computer control. The reflected fluorescence light from the sample was collected through an analyzer, followed by an imaging spectrograph (see Fig. 1(c)) to a modulated image intensifier and detected with a cooled charge-coupled device (CCD) camera. The spectrograph was calibrated according to Ref. [11]. The LED and the intensifier gain were modulated at the same frequency (60 MHz). A series of images were acquired while adjusting the relative phase delay between the intensifier and the LED. Two sets of measurements were made with the controlled polarization rotator oriented either 0° or 90° relative to the analyzing polarizer. To validate the accuracy of the imaging system for the measurement of wavelength-dependent anisotropy, experimental data were obtained from a series of bulk glycerol/water and rhodamine 6G mixtures.

The two-dimensional (2D) maps of the spectrum and anisotropy from the mixtures of 59% glycerol and 10-μmol/L rhodamine 6G are shown in Fig. 2, where the parallel axis is the wavelength λ and the perpendicular axis is the slit width of spectrograph x. As the solution of 10-μmol/L rhodamine 6G mixed with 91% glycerol and deionized water is a high viscosity liquid, the rotation of

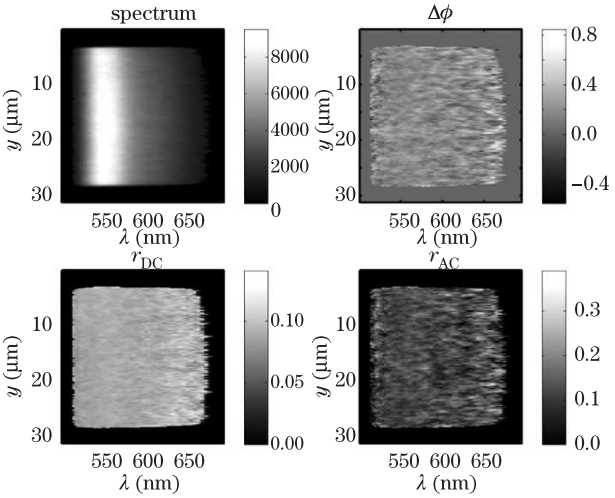

Fig. 2. 2D maps of the spectrum and time-resolved anisotropy measured from the mixtures of 59% glycerol and 10-μmol/L rhodamine 6G. It is noted that the light intensities are threshold and only limited region (510 nm $< \lambda <$ 670 nm) is chosen to be displayed.

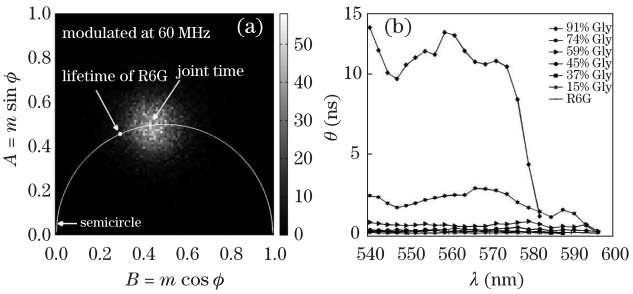

Fig. 3. Fluorescence joint time and fluorescence rotational correlation time. (a) Polarized phasor histograms of the fluorescence lifetime and joint time of 10-μmol/L rhodamine 6G (R6G) solutions mixed with 91% glycerol (Gly); for $r_\infty = 0$, $\triangle p = p_0 r_0 \exp(-n/\xi)$, according to Eq. (4), is a single exponential decay with the time constant ξ, represented by a circular histogram distribution on the semicircle in the phasor space. (b) Relation between the concentration of Gly and the fluorescence rotational correlation time. It is noted that the light intensities are threshold and only limited region (540 nm $< \lambda <$ 600 nm) is chosen to be displayed.

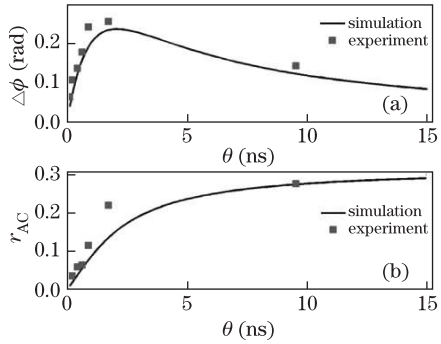

Fig. 4. Relation between the fluorescence rotational correlation time and the time-resolved anisotropy: (a) θ and $\triangle\phi$; (b) θ and r_{AC}.

relatively small molecule of rhodamine 6G is impeded by its circumstance. Its polarized phasor plot deduced from Eq. (4) is shown in Fig. 3(a), where the histogram of the fluorescence joint time is a circular Gaussian distribution with the center $\xi = 2.84$ ns located on the semicircle, and it hints that the physics of the fluorescence joint time is single exponential decay. According to Eq. (2), the corresponding rotational correlation time is calculated to be $\theta = 12.51$ ns. By the same way above, the rotational correlation time is calculated for 10-μmol/L rhodamine 6G solutions mixed with 0%, 15%, 37%, 45%, 59%, 74%, and 91% glycerol and deionized water, and the wavelength-dependant relations of the viscosities and the rotational correlation time for the whole series of the solutions are shown in Fig. 3(b). They follow a nearly linear relation in the logical plot, corresponding to Eq. (7). The relation between the rotational correlation time θ and the modulated phase delay $\triangle\phi$ is shown in Fig. 4(a), which pronounces a hump; while the relation between the rotational correlation time θ and the time-resolved anisotropy r_{AC} is shown in the Fig. 3(b), which pronounces nonlinear rising. Both relations conform to the theoretical model[1,2].

The fluorescence time-resolved anisotropy can be evaluated by the parameters: r_{DC}, r_{AC}, $\triangle\phi$, θ[3], and the new parameter ξ. Among them, the dynamic ranges of the fluorescence rotational correlation time θ and fluorescence joint time ξ are much larger than others. However, unlike fluorescence lifetime, it is impossible to present the rotational correlation time in the phasor space, and this impedes its application. Because the fluorescence joint time ξ can be transformed to the phasor space, it is particularly useful to distinguish multiple fluorescence cycles using the concept of trajectories and mapping between the phasor space and intensity imaging[12]. It is the most suitable parameter to weigh for the macromolecule dynamics.

In conclusion, we have discussed different methods to analyze the fluorescence time-resolved anisotropy, and proven that the phasor approach could be widely applicable without prerequisite, no matter the measurement is done in the frequency domain or in the time domain.

This work was partially supported by the Engineering and Physical Sciences Research Council, UK, under a Life Science Interface Grant (No. EP/E013422/1) and the State 211 Project of China (YueFaGai 2009 (432)). The authors are grateful to Dr. Q. S. Hanley at Nottingham Trent University, UK, for his encouragement and helpful discussions.

References

1. J. R. Lakowicz, *Principles of Fluorescence Spectroscopy* (Springer, New York, 2006).
2. T. Yun, N. Zeng, W. Li, and H. Ma, Acta Opt. Sin. (in Chinese) **29,** 1926 (2009).
3. A. H. A. Clayton, Q. S. Hanley, D. J. Arndt-Jovin, V. Subramaniam, and T. M. Jovin, Biophys. J. **83,** 1631 (2002).
4. J. Siegel, K. Suhling, S. Leveque-Fort, S. E. D. Webb, D. M. Davis, D. Phillips, Y. Sabharwal, and P. M. W. French, Rev. Sci. Instrum. **74,** 182 (2003).
5. K. Suhling, J. Siegel, P. M. P. Lanigan, S. Leveque-Fort, S. E. D. Webb, D. Phillips, D. M. Davis, and P. M. W. French, Opt. Lett. **29,** 584 (2004).
6. Y. Zhou, J. M. Dickenson, and Q. S. Hanley, J. Microsc.-Oxford **234,** 80 (2009).
7. Y. Zhou, L. Wu, Q. Wang, and Y. Wang, J. Fluoresc. doi: 10.1007/s10895-010-0683-4 (2010).
8. D. M. Jameson, E. Gratton, and R. D. Hall, Appl. Spectrosc. Rev. **20,** 55 (1984).
9. A. H. A. Clayton, Q. S. Hanley, and P. J. Verveer, J. Microsc.-Oxford **213,** 1 (2004).
10. A. H. A. Clayton, J. Microsc.-Oxford **232,** 306 (2008).
11. Y. Li, Y. Zhang, J. Liu, Z. Rong, L. Zhang, and Y. Zhang, Acta Opt. Sin. (in Chinese) **29,** 41 (2009).
12. M. A. Digman, V. R. Caiolfa, M. Zamai, and E. Gratton, Biophys. J. **94,** L14 (2008).